IEEE Access
Multidisciplinary | Rapid Review | Open Access Journal

Received 17 July 2023, accepted 9 August 2023, date of publication 14 August 2023, date of current version 17 August 2023.

*Digital Object Identifier 10.1109/ACCESS.2023.3305278*

RESEARCH ARTICLE

# An Investigation of Process Variations and Mismatch Characteristics of Vertical Bipolar Junction Transistors

**XIAONIAN LIU AND ZICHEN YANG**
School of Physics and Electronics, Hunan Normal University, Changsha 410081, China

Corresponding author: Xiaonian Liu (xiaonian@hunnu.edu.cn)

This work was supported in part by the National Natural Science Foundation of China under Grant 62204083, and in part by the Youth Fund of Education Department of Hunan Province under Grant 21B0057.

**ABSTRACT** Bipolar junction transistors (BJT) are widely used integrated devices for analog circuits. For most of analog applications, the process variation and the match performance of BJT pairs are critical for the circuit design. Vertical BJT device has advantages of current gain stability and high carriers collect efficiency over lateral BJT device. This work investigates the process variation, mismatch characteristics and related data distribution of 0.11 $\mu$m process vertical BJT devices throughly. Experiment data indicates that bigger devices have smaller electrical dispersion and better match characteristics than smaller devices of the same type. The distribution of electrical parameters does not conform with the typical Gaussian distribution. The standard deviation of the electrical parameter difference of matched device pairs is inversely proportional to the square root of emitter area. Generally, the matching properties of 3.3 V BJT devices are better than their 1.5 V counterparts, the PNP BJT devices matches better than their NPN counterparts with the same operating voltage and geometry size. The mismatch ratio is not located at the exact zero point but slightly deviates from the center zero point. The die location does not show significant impact on the statistical performance of vertical BJT devices. Electrical parameters of the same type and different bias point have strong statistical correlations. These investigated properties of process variation and mismatch characteristics is helpful for the analog circuit design which requires high accuracy matched vertical BJT device pairs.

**INDEX TERMS** Bipolar junction transistor (BJT), process variation, mismatch.

## I. INTRODUCTION

Throughout decades development of semiconductor technology and integrated circuits (IC), bipolar junction transistor (BJT) plays a key role in analog, radio frequency (RF) circuits, high speed digital circuits and power control circumstances. The wide application of BJT benefits from its excellent properties of high linearity, high switch efficiency and high current gain [1], [2], [3], [4]. The heterojunction bipolar transistors (HBT) have advantages over conventional BJT devices like high injection efficiency, high speed and low noise [5], [6], [7], [8]. While, it also suffers from its drawbacks such as the interface quality [9], relatively high cost, electrothermal effects [10] and the poor compatibility with Si CMOS technology. Thus, conventional BJT devices has its own application occasions.

The physical implementations of integrated BJT devices are lateral and vertical structures. Lateral BJTs suffers from beta roll off effect at high and low collector current situation. The current gain decays with low collector current physically originates from the surface combination of these surface carriers of base node of BJT [11]. Vertical BJT overcomes this short back with its contact surface of emitter and base all beneath the silicon surface. Thus, vertical structure is a prior implementation for the BJTs with stable and high current gain [12], [13], [14], [15].

Integrated manufacturing process has a poor absolute conformance and stability [16]. Some key electrical parameters

The associate editor coordinating the review of this manuscript and approving it for publication was Sneh Saurabh.

of devices can varies by several or even several tens of percentages due to process variations. Roughly speaking, these variations can be classified into 2 types: the interdie variation between different dies and the intradie variation within the same single die [17]. The interdie variation can be induced by the wafer-to-wafer variation, the lot-to-lot variation and the die-to-die gradient variation in the same wafer. The intradie variation are caused by the random process fluctuation, the gradient effects within die, the across chip linewidth variation (ACLV) and the across field linewidth variation (AFLV) which induced by lithography [18], [19], [20], [21], [22]. Monitoring circuits are developed for the on-chip process variation detection [23], [24].

If the performance of circuit highly relies on the absolute feature values of a single transistor, the circuit will suffer from the huge interdie variation. Thus, the performance of a well-designed circuit depends on the differential value of a matched pair. This kind of circuits becomes robust to interdie variation and only relies on the much smaller differential mismatch variation. The objective of matched pair to eliminate interdie variation is depicted in Fig. 1. The match pair method are widely used in analog circuits [3], [14] such as current mirrors [25], band-gap voltage [26], sense amplifiers [27], voltage dividers, fully differential analog circuits [28] and feedback networks. Technical methods in circuit level are also studied to eliminate the negative impact of mismatch issue in analog circuits. A compensation method has been proposed to eliminate the mismatch in sub-threshold current mirrors [29]. A ring oscillator (RO) based circuit has been designed to detect the MOSFETs' threshold voltage variation [30].

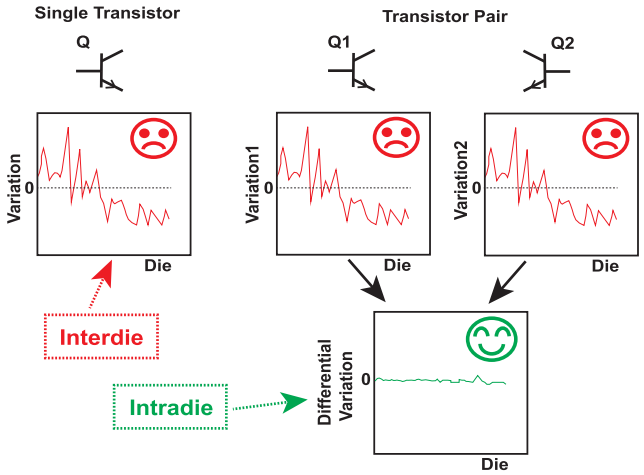


**FIGURE 1.** The intradie variation of a match pair transistors is much smaller than the interdie of a single transistor.

The process variation and mismatch of MOSFET devices have been studied throughly [16], [31], [32], even in nano-scale process node [33], [34] and nanowire MOSFETs [35]. A simulation study has been performed to evaluate the fin angle variation induced threshold voltage shift in FinFET devices [36]. The process variation studies of HBT devices focus on their high-frequency figure of merits [37], [38]. The modeling of process variation and mismatch issue in circuit simulation is researched [39], [40], [41], [42], [43], [44], [45]. Physics based BJT model has been developed for the modeling of electrical behaviors of BJT devices [46], [47], [48]. The base width modulation effect [49] and mechanical stress effect [50] of BJT devices has been studied. The NPN BJT mismatch dependence on the devices' layout orientation [51] has been researched.

This work investigates the process variations and mismatch characteristics of vertical BJT device pairs. The average value, relative standard deviation and its distribution, mismatch ratio and matched device pairs' electrical parameter distribution, the influence of die location, the correlations of different electrical parameters are presented and discussed.

This article is organized as follows. In section II, the experiment setting, devices' properties and measured electrical values are introduced. The properties of BJT devices includes the layout, doping polar types, operating voltages and geometry sizes. In section III, the statistical properties of process variations and mismatch characteristics of BJT devices including the data and distribution of deviation and mismatch ratio are illustrated and discussed. The dependency on die location and the correlations of different electrical parameters are studied. The conclusion is given in section IV.

## II. EXPERIMENT DETAILS

Tested vertical BJT devices were fabricated by 0.11 $\mu$m 4-poly 7-metal low power embedded superflash process. The diameter of based wafers are 200 mm. On wafer mapping test was carried out by a Cascade machine which controlled by the Nucleus software. Agilent 4156C parameter analyzer was used for the electrical data measurement at room temperature. The doping polar types, operating voltages, geometry sizes of vertical BJT devices are listed in Table 1. There are 12 combinations of these 3 properties of vertical BJT devices. Each type among 12 combinations of vertical BJT been designed a matched pair in every single die.

**TABLE 1.** Properties of vertical BJT devices.

| Properties | Values |
|---|---|
| Doping polar | NPN and PNP |
| Operating voltage $V_{CC}$ | 1.5 V and 3.3 V |
| Emitter size ($A_e$) and base size ($A_b$) | $A_e = 10 \times 10\mu m^2, A_b = 16 \times 16\mu m^2$<br>$A_e = 5 \times 5\mu m^2, A_b = 11 \times 11\mu m^2$<br>$A_e = 2 \times 2\mu m^2, A_b = 8 \times 8\mu m^2$ |

These devices are fabricated in 13 wafers namely #1, #4, #5, #7, #8, #10, #11 in lot A140.1 and #7, #8, #9, #10, #11, #12 in lot A044.1. Each wafer has 30 dies, coordinates and corresponding locations of these dies are illustrated in Fig. 2.

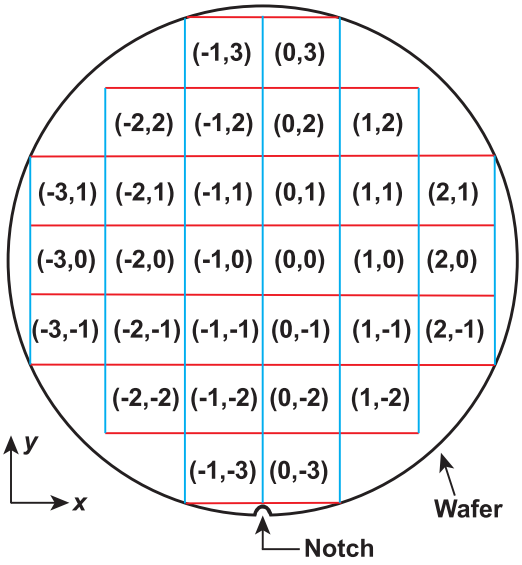


**FIGURE 2.** The coordinates and corresponding locations of 30 dies in the wafer.

**TABLE 2.** Measured key electrical parameters of vertical BJT devices.

| Symbol | Quantity |
|---|---|
| $\beta(0.6)$ and $\beta(0.7)$ | the current gain at $\lvert V_{be}\rvert$ =0.6 V and 0.7 V |
| $I_e(0.6)$ and $I_e(0.7)$ | the emitter current at $\lvert V_{be}\rvert$ =0.6 V and 0.7 V |
| $I_b(0.6)$ and $I_b(0.7)$ | the base current at $\lvert V_{be}\rvert$ =0.6 V and 0.7 V |
| $I_c(0.6)$ and $I_c(0.7)$ | the collector current at $\lvert V_{be}\rvert$ =0.6 V and 0.7 V |
| $V_{be}(10)$, $V_{be}(100)$ and $V_{be}(1000)$ | the base-emitter voltage when the base current $I_b$ satisfies $\lvert I_b\rvert$ =10 nA, 100 nA and 1000 nA |

For NPN BJT devices, $|V_{be}| = +V_{be}$, $|I_b| = +I_b$.

For PNP BJT devices, $|V_{be}| = -V_{be}$, $|I_b| = -I_b$.

To evaluate the process variation and mismatch, some key electrical values of vertical BJT devices are measured, these electrical parameters are listed as Table 2.

The physical structure and device layout of vertical BJT devices are different from that of their lateral counterpart. The cross section view and the layout of vertical BJT devices are shown in Fig. 3. The PNP devices are constituted by P+ doped active area as emitter, N-type well (Nwell) as base and P-type substrate (Psub) as collector. The NPN devices are constituted by N+ doped active area as emitter, P-type well (Pwell) as base and Nwell/deep Nwell (DNW) as collector. For both 2 types of devices, the emitter junction and collector junction are all constructed vertically beneath the silicon surface. The emitter is surrounded by the base and the base is surrounded by the collector, which is helpful for the collector efficiency. The emitter is a small heavy doped area at center, which surrounded by the base vertical direction and by the shallow trench isolation (STI) in horizontal direction. The outer circle are contacts that connect to the collector which is Psub for PNP devices and DNW for NPN devices.

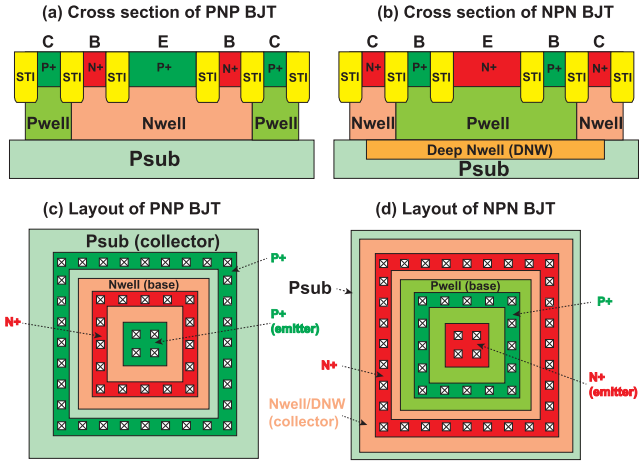


**FIGURE 3.** The cross section view and the layout of vertical PNP and NPN BJT devices.

## III. PROCESS VARIATION AND MISMATCH

There are total 12 kinds of BJT devices with 2 doping polar types, 2 operating voltages and 3 geometry sizes. Matched device pairs for each kind of BJT device are fabricated in 30 dies on each of 13 wafers which belongs to 2 lots. For each single device and device pairs, we have measured 11 electrical values which is listed in Table 2. Here we investigate the average and relative standard deviation of all devices, the electrical values' distribution of different devices, the mismatch ratios' distribution of different devices, the statistical dependency on the die locations, and the correlations between different electrical values.

### A. AVERAGE AND RELATIVE STANDARD DEVIATION

For these all 12 kinds of BJT devices, the average of measured values are listed in Table 3. It can be seen that the emitter current $I_e$ at emitter junction voltage $V_{be}$ = 0.7 V is much higher than their counterpart when $V_{be}$ = 0.6 V. The emitter junction turn-on voltage $V_{be}$ is around 0.6-0.7 V. To estimate the turn-on voltage, the emitter voltage $V_{be}$ when the base current of 10 nA, 100 nA and 1000 nA are measured and denoted as $V_{be}(10)$, $V_{be}(100)$ and $V_{be}(1000)$. It indicates that the $V_{be}$ values of devices with larger geometry size is smaller than that of devices with smaller geometry size. The process induced deviation of devices are also depends on the geometry size.

In Table 4, the relative standard deviations of turn-on voltage $V_{be}$ in percentage are illustrated. Roughly speaking, the relative standard deviation of bigger device is smaller than that of smaller device with the same operating voltage and doping polar type. The relative standard deviation difference between devices of $A_e = 10 \times 10\mu m^2$ and $A_e = 5 \times 5\mu m^2$ is much smaller than the difference between $A_e = 5 \times 5\mu m^2$ and $A_e = 2 \times 2\mu m^2$. The standard deviation is mainly caused by the random fluctuation issues of process and devices. This random irregularity can be classified as peripheral variation which is proportional to the perimeter of device and areal

**TABLE 3.** The average values of all kinds of devices.

| $V_{CC}$ | Doping | $A_e(\mu m^2)$ | $I_e(0.6)$ | $I_b(0.6)$ | $I_c(0.6)$ | $I_e(0.7)$ | $I_b(0.7)$ | $I_c(0.7)$ | $V_{be}(10)$ | $V_{be}(100)$ | $V_{be}(1000)$ |
|---|---|---|---|---|---|---|---|---|---|---|---|
| 1.5 | NPN | $10 \times 10$ | -0.266 | 0.0329 | 0.237 | -12.57 | 1.46 | 11.20 | 0.559 | 0.621 | 0.683 |
| 1.5 | NPN | $5 \times 5$ | -0.0729 | 0.00935 | 0.0644 | -3.46 | 0.403 | 3.10 | 0.593 | 0.655 | 0.717 |
| 1.5 | NPN | $2 \times 2$ | -0.0146 | 0.00208 | 0.0127 | -0.690 | 0.0816 | 0.617 | 0.635 | 0.698 | 0.761 |
| 1.5 | PNP | $10 \times 10$ | 0.175 | -0.0614 | -0.116 | 8.34 | -2.89 | -5.51 | -0.543 | -0.603 | -0.664 |
| 1.5 | PNP | $5 \times 5$ | 0.0480 | -0.0170 | -0.0317 | 2.30 | -0.808 | -1.52 | -0.576 | -0.637 | -0.698 |
| 1.5 | PNP | $2 \times 2$ | 0.00967 | -0.00362 | -0.00620 | 0.462 | -0.170 | -0.300 | -0.617 | -0.678 | -0.739 |
| 3.3 | NPN | $10 \times 10$ | -0.293 | 0.0279 | 0.268 | -13.82 | 1.25 | 12.66 | 0.564 | 0.625 | 0.687 |
| 3.3 | NPN | $5 \times 5$ | -0.0786 | 0.00783 | 0.0717 | -3.75 | 0.344 | 3.45 | 0.598 | 0.660 | 0.722 |
| 3.3 | NPN | $2 \times 2$ | -0.0152 | 0.00170 | 0.0137 | -0.723 | 0.0689 | 0.663 | 0.640 | 0.703 | 0.766 |
| 3.3 | PNP | $10 \times 10$ | 0.175 | -0.0614 | -0.116 | 8.34 | -2.89 | -5.51 | -0.543 | -0.603 | -0.664 |
| 3.3 | PNP | $5 \times 5$ | 0.0541 | -0.0172 | -0.0377 | 2.59 | -0.819 | -1.81 | -0.576 | -0.637 | -0.697 |
| 3.3 | PNP | $2 \times 2$ | 0.0109 | -0.00372 | -0.00735 | 0.521 | -0.175 | -0.354 | -0.617 | -0.677 | -0.738 |

The unit of voltage is V and the unit for current is μA.

**TABLE 4.** The relative standard deviation of turn-on voltage $V_{be}$.

| $V_{CC}$ | Doping | $A_e(\mu m^2)$ | $V_{be}(10)$ | $V_{be}(100)$ | $V_{be}(1000)$ |
|---|---|---|---|---|---|
| 1.5 | NPN | $10 \times 10$ | 0.1037 | 0.0921 | 0.0826 |
| 1.5 | NPN | $5 \times 5$ | 0.1132 | 0.1009 | 0.0908 |
| 1.5 | NPN | $2 \times 2$ | 0.1577 | 0.1442 | 0.1351 |
| 1.5 | PNP | $10 \times 10$ | 0.1013 | 0.0910 | 0.0829 |
| 1.5 | PNP | $5 \times 5$ | 0.1037 | 0.0912 | 0.0815 |
| 1.5 | PNP | $2 \times 2$ | 0.1256 | 0.1139 | 0.1053 |
| 3.3 | NPN | $10 \times 10$ | 0.0964 | 0.0855 | 0.0780 |
| 3.3 | NPN | $5 \times 5$ | 0.0987 | 0.0880 | 0.0803 |
| 3.3 | NPN | $2 \times 2$ | 0.1241 | 0.1099 | 0.1037 |
| 3.3 | PNP | $10 \times 10$ | 0.1000 | 0.0893 | 0.0813 |
| 3.3 | PNP | $5 \times 5$ | 0.0985 | 0.0890 | 0.0802 |
| 3.3 | PNP | $2 \times 2$ | 0.1146 | 0.1033 | 0.0949 |

The values of table is in percentage (%).

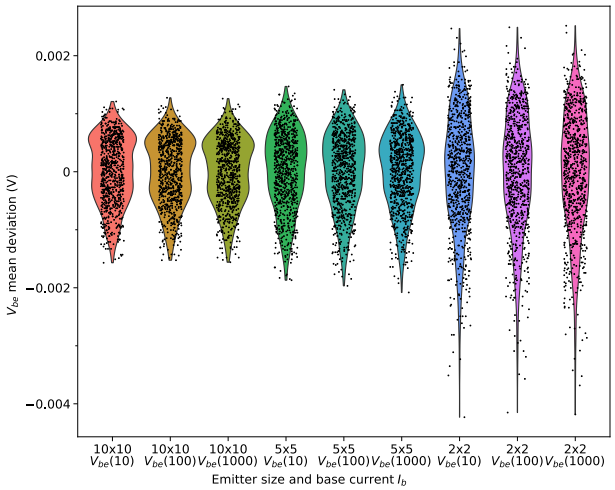


**FIGURE 4.** The turn-on voltage $V_{be}$ distribution of 1.5 V NPN BJT devices.

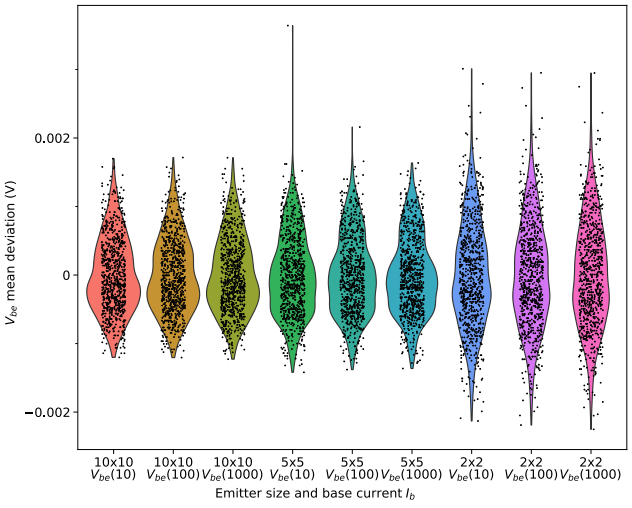


**FIGURE 5.** The turn-on voltage $V_{be}$ distribution of 1.5 V PNP BJT devices.

variation which is determined by the area of device. Most of random fluctuation issues are areal variations, which can be modeled by [14]

$$s = m\sqrt{\frac{k}{2A_{active}}}. \tag{1}$$

where $s$ and $m$ is the standard deviation and average value of electrical parameter of devices with the active area $A_{active}$, the coefficient $k$ relies on the physical origin of process variation.

### B. ELECTRICAL PARAMETERS' DISTRIBUTION

The standard deviation can reflect the process deviation to some extent. While this single value is inadequate to describe the distribution of electrical parameters. Thus, it is essential to illustrate the detail data distribution of devices' electrical parameters. Fig. 4, 5, 6 and 7 are the mean deviation distribution of turn-on voltage $V_{be}$ for different types of BJT devices with varies geometry size.

The mean deviation is the deviation of each statistical value from the average value. The mean deviation distribution of all devices does not obey the typical Gaussian distribution. The distribution curve is not a single peak value in average value, but 2 local peak values located at both sides of center average value for 2 types of bigger devices. Most of these deviations falling within the range of ±0.002 V. The deviation of devices with emitter area $A_e = 10 \times 10\mu m^2$ and $A_e = 5 \times 5\mu m^2$ are

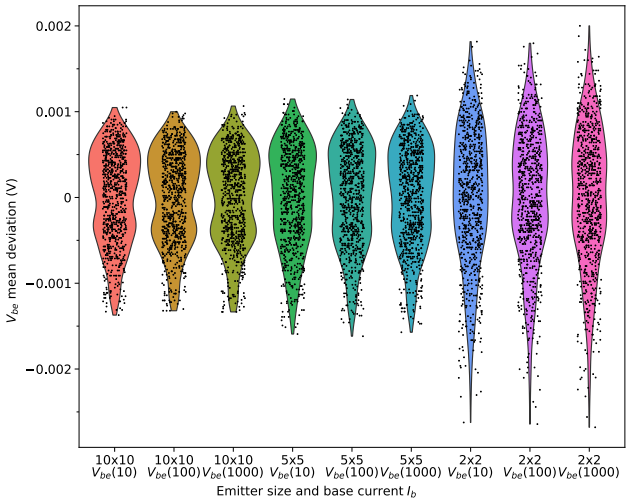


**FIGURE 6.** The turn-on voltage $V_{be}$ distribution of 3.3 V NPN BJT devices.

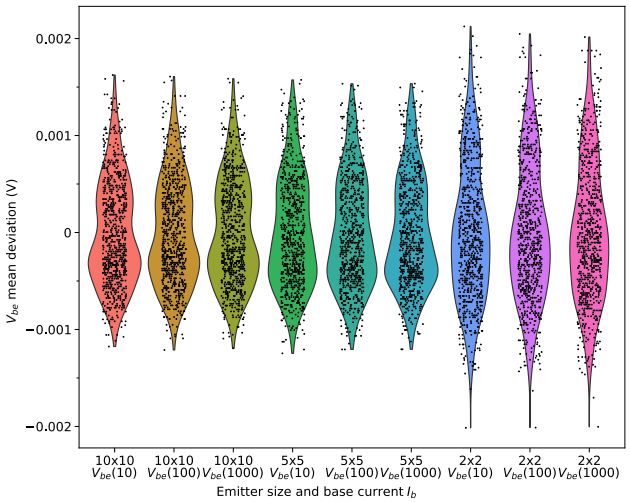


**FIGURE 7.** The turn-on voltage $V_{be}$ distribution of 3.3 V PNP BJT devices.

nearly the same, while the deviation of devices with emitter area $A_e = 2 \times 2\mu m^2$ is much higher than their larger counterparts. This is agree with the relative standard deviation values listed in Table 4. Another phenomenon should be mentioned is that for NPN BJT devices, these electrical parameter data with positive mean deviation is more concentrated that that of negative mean deviation; for PNP BJT devices, things are on the contrary. In other words, for both types of BJT devices, the turn-on voltage $V_{be}$ data with higher absolute current value tend to be more concentrated.

It is observed that this two peaks distribution can be roughly expressed as the sum of 2 Gaussian density function. In Fig. 8, the distribution density of $V_{be}(1000)$ values of 3.3 V NPN devices with $A_e = 10 \times 10\mu m^2$ are fitted as the sum of 2 Gaussian functions with different expected values ($\mu_1$ and $\mu_2$), standard deviations ($\sigma_1$ and $\sigma_2$) and appropriate weight ratio ($\lambda_1$ and $\lambda_2$).

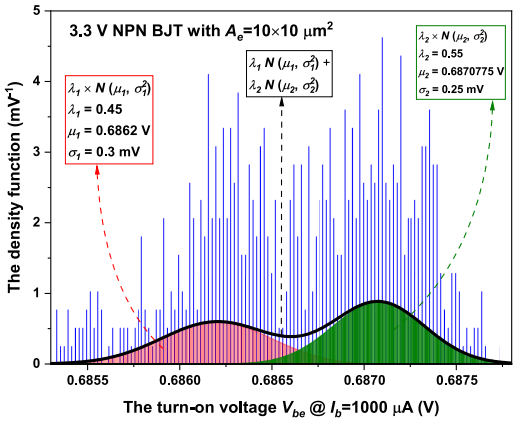


**FIGURE 8.** A two Gaussian distribution fitting of the turn-on voltage $V_{be}$ ($@I_b$ =1000 nA) of 3.3 V NPN BJT devices.

### C. MISMATCH RATIO

As is mentioned before, to avoid the high absolute process variation of interdie and even intradie, matched devices pairs are designed to improve the performance of analog circuits. To evaluate the mismatch of vertical BJT devices, each device in this work has its matched device at nearby location. There is one pair of matched devices in each die for every kind of BJT devices with specified operating voltage, doping polar type and geometry size. Thus, there are $30 \times 13 = 390$ matched pairs for each kind of BJT devices.

The standard deviation of 2 closely placed matched transistor pair $\sigma\ (\Delta P)$ is inversely proportional to the square root of transistor's active area [52], [53], [54]

$$\sigma\ (\Delta P) = \frac{\sqrt{a_p}}{\sqrt{A_{active}}}. \tag{2}$$

where $a_p$ is a process-dependent fitting constant and $A_{active}$ is the active area. For BJT devices, the active area $A_{active}$ is taken as the emitter area $A_e$.

Fig. 9 illustrates the relationship between the standard deviation of $V_{be}$ (10) and the emitter active area $A_{active}$. It can be seen that the standard deviation of $V_{be}$ (10) is inversely proportional to the square root of emitter active area $A_{active}$. This is agree with the linear relations in (2). Fig. 9 also tells that for vertical BJT devices with the same geometry size, BJT devices with operating voltage $V_{CC} = 1.5$ V is worse than that of $V_{CC} = 3.3$ V, NPN type BJT mismatch is worse than PNP type.

The standard deviation can roughly evaluate the degree of mismatch dispersion. The detail data distribution is essential for the mismatch distribution morphology study. Fig. 10 and Fig. 11 are scatter and spectral density curves of mismatch data.

In Fig. 10, each device pair is denoted as device A and device B of the same kind. The horizontal axis is the turn-on voltage $V_{be}$ of device A at the base current $|I_b| = 100$ nA. The vertical axis is the same value of device B. Graphs (a), (b) and (c) are for 1.5 V NPN devices with different emitter area. Graph (d) is for 1.5 V PNP devices with emitter area

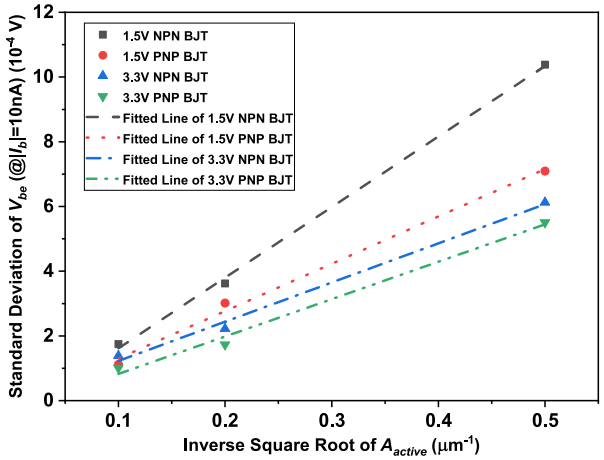


**FIGURE 9.** The turn-on voltage (@$|I_b|$ =10 nA) mismatch ratio dependency on the inverse square root of active area $A_{active}$.

$A_e = 10 \times 10\mu m^2$. For perfectly matched device pairs, all data should fall on the centerline $B = A$. Actual measured data spreads around this centerline. We define a minimum number $\epsilon$, this $\epsilon$ satisfies (3) for all matched device pairs of the same kind.

$$\left|\frac{B-A}{A}\right| = \left|\frac{B}{A} - 1\right| \leq \epsilon. \tag{3}$$

Thus, all data are falling on the region between parallel lines $B = (1 \pm \epsilon) \cdot A$. For 1.5 V NPN devices, the $\epsilon$ values are 0.73‰, 1.7‰ and 5.7‰ for different geometry sizes. It indicates that devices with larger geometry size has better matching performance than smaller devices of the same type. For 1.5 V PNP devices with $A_e = 10 \times 10\mu m^2$, the $\epsilon$ value is 0.66‰, which is smaller than 0.73‰ of 1.5 V NPN device with the same active area. This is agree with the trend in Fig. 9.

The Fig. 11 is the mismatch ratio distribution for 4 types of devices with $A_e = 10 \times 10\mu m^2$ and $A_e = 2 \times 2\mu m^2$. The mismatch ratio $\delta$ for device pair (A, B) is defined as

$$\delta = \frac{difference\ of\ A\ and\ B}{average\ of\ A\ and\ B} = 2 \cdot \frac{B-A}{B+A}. \tag{4}$$

For each graph in Fig. 11, the left half is for NPN devices and right half for PNP devices. Compare (a) and (b) or (c) and (d), one can see that the mismatch of smaller geometry size is much worse than bigger devices of the same type. Compare (a) and (c) or (b) and (d), one can see that the mismatch ratio dispersion of 3.3 V devices is slightly better than 1.5 V devices with the same doping type and geometry size. In each graph, one can see that the $V_{be}$ mismatch ratio for higher current is better than that of low current. It also indicates that the mismatch ratio dispersion of NPN devices are worse than that of PNP devices. One thing also should be mentioned is that the peak value of mismatch ratio distribution curve is not located at zero, but slightly deviate from zero.

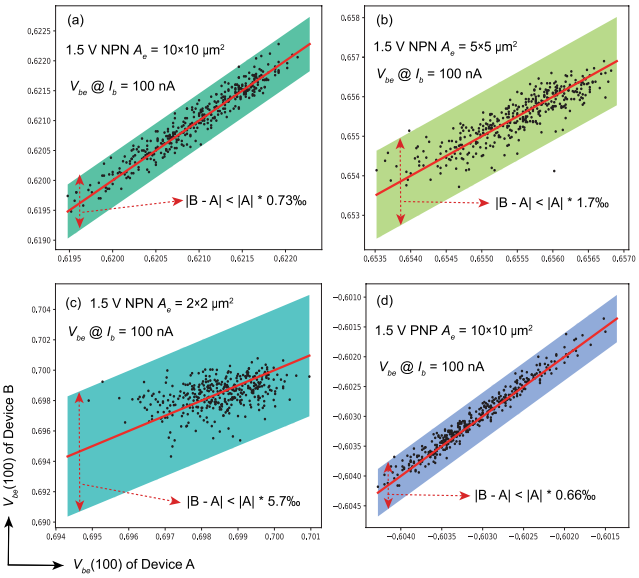


**FIGURE 10.** The scatters of turn-on voltage $V_{be}$ (@ $|I_b|$ =100 nA) of matched BJT device pairs.

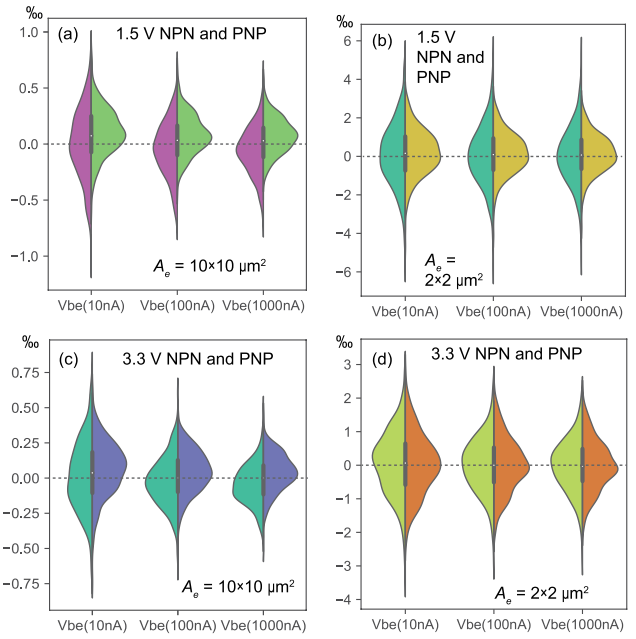


**FIGURE 11.** The turn-on voltage mismatch ratio distribution of different BJT device pairs.

### D. DIE LOCATION

The statistical and mismatch dependency on device properties are studied. It is also essential to investigate their relationship on the die location. Fig. 12 illustrates the average value (in V), standard deviation (in mV) and mismatch ratio (in ‰) of $V_{be}(10)$ of 1.5 V NPN BJT devices with emitter area $A_e = 10 \times 10\mu m^2$.

Fig. 12 (a) shows that the average values of $V_{be}(10)$ have no significant statistical relationships on the die location on wafer. On this specific graph, 2 center dies (-1, 0) and (0, 0) tends to get medium value of $V_{be}(10)$; the dies that neither

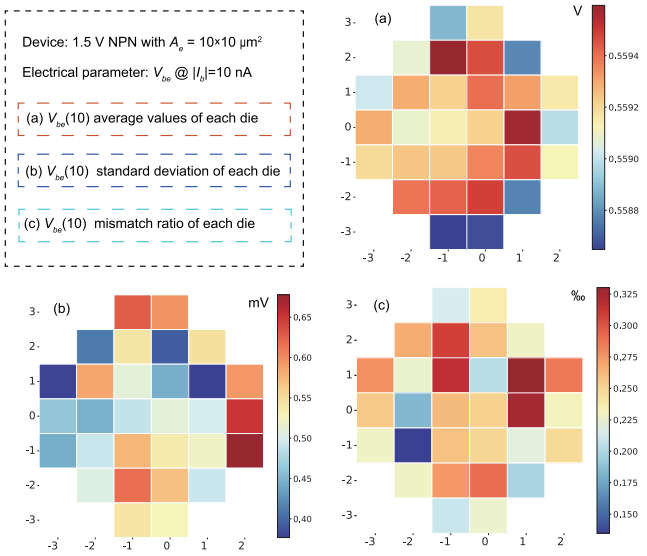


**FIGURE 12.** The (a) average value, (b) standard deviation and (c) mismatch ratio of turn-on voltage $V_{be}$ (@$|I_b|$ =10 nA) for 1.5 V NPN BJT devices with $A_e = 10 \times 10\mu m^2$.

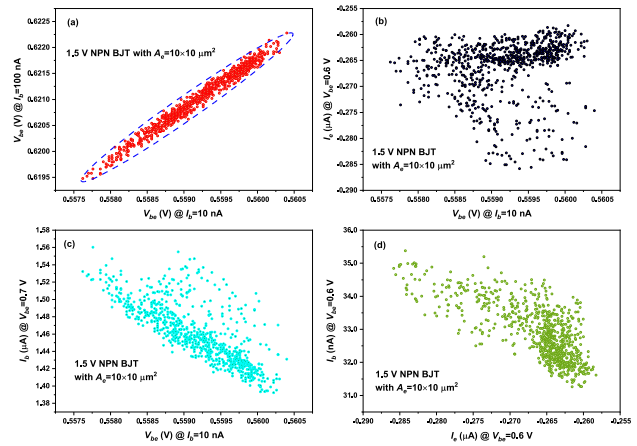


**FIGURE 13.** The correlations of different electrical parameters of 1.5 V NPN BJT devices with $A_e = 10 \times 10\mu m^2$.

central nor peripheral tends to get a higher value of $V_{be}(10)$; and the peripheral dies that far from the center is more likely to get a lower value of $V_{be}(10)$.

Fig. 12 (b) and (c) tells that the standard deviation and the mismatch ratio of $V_{be}(10)$ both have no significant statistical relationships on the die location. Compare graph (b) and (c), it can be found that the deviation from average value and the mismatch ratio of matched pairs has no necessary statistical connection. The lowest deviation and the highest mismatch ratio belong to the same die (1, 1). The highest deviation and a medium mismatch ratio overlay on the die (2, -1). The die (-2, -1) has the lowest mismatch ratio but a medium value of deviation.

### E. CORRELATIONS OF ELECTRICAL PARAMETERS

Hereto the statistical and mismatch characteristics of certain electrical parameter are discussed, especially the turn-on voltage $V_{be}$. Fig. 13 gives the correlations of some different electrical parameters of 1.5 V NPN BJT devices with emitter area $A_e = 10 \times 10\mu m^2$.

Fig. 13 (a) indicates that the turn-on voltage $V_{be}$ at base current $I_b = 10$ nA and $I_b = 100$ nA conforming to a perfect linear relationship. The subgraph (b) tells that the turn-on voltage $V_{be}(10)$ has no obvious correlation with the emitter current $I_e(0.6)$. The subgraph (c) indicates that devices with higher positive $V_{be}(10)$ deviation is more likely to have a lower $I_b(0.7)$ value. Similarly, the subgraph (d) shows a weak positive correlation between the absolute value of $I_e(0.6)$ and $I_b(0.6)$.

## IV. CONCLUSION

The process variation and mismatch characteristics is critical for the performance of analog circuits. This work studies the process variation, mismatch ratio and related data distribution of 0.11 $\mu$m process node vertical BJT devices throughly. It is found that devices of smaller geometry size have greater statistical dispersion; the distribution of data deviation does not conform with the typical Gaussian distribution but can be roughly expressed as the sum of 2 Gaussian distribution with proper weight ratio. For both NPN and PNP type BJT devices, the turn-on voltage data of higher absolute current value are more concentrated. The mismatch values' standard deviation of vertical BJT devices with different geometry size is inversely proportional to the square root of their emitter area. Roughly speaking, the match performance of higher operating voltage devices are better than that of lower operating voltage and PNP BJT devices' matching are better than their NPN counterparts. The peak of mismatch ratio distribution is not exactly located at zero. The die location has little impact on the statistical properties of devices. The same type of electrical parameters of different bias have significant statistical correlations. This work is meaningful for analog circuits which requires accurate match properties of vertical BJT device pairs.

## REFERENCES

[1] T. H. Ning, "History and future perspective of the modern silicon bipolar transistor," *IEEE Trans. Electron Devices*, vol. 48, no. 11, pp. 2485–2491, Nov. 2001.

[2] D. A. Neamen, *Microelectronics: Circuit Analysis and Design*, 4th ed. New York, NY, USA: McGraw-Hill, 2009.

[3] B. Razavi, *Design of Analog CMOS Integrated Circuits*, 2nd ed. New York, NY, USA: McGraw-Hill, 2018.

[4] S. Pande, S. Balanethiram, A. K. Singh, M. Gupta, B. Umapathi, H. S. Jatana, N. Mohapatra, and A. Chakravorty, "Development of low-cost silicon BJT technology and modeling," in *Proc. 5th IEEE Int. Conf. Emerg. Electron. (ICEE)*, Nov. 2020, pp. 1–4.

[5] A. Zhang and J. Gao, "Emitter-length scalable small signal and noise modeling for InP heterojunction bipolar transistors," *IEEE Access*, vol. 7, pp. 13939–13944, 2019.

[6] S. Wahid and Md. K. Alam, "Efficiency enhancement of perovskite solar cells using heterojunction bipolar transistor configuration," *IEEE Trans. Electron Devices*, vol. 67, no. 2, pp. 552–557, Feb. 2020.

[7] Y. Shiratori, T. Hoshi, and H. Matsuzaki, "InGaP/GaAsSb/InGaAsSb/InP double heterojunction bipolar transistors with record ft of 813 GHz," *IEEE Electron Device Lett.*, vol. 41, no. 5, pp. 697–700, May 2020.

[8] J. Suarez and M. Shur, "Terahertz diagnostics of SiGe heterojunction bipolar transistors," in *Proc. Int. Conf. Electr., Comput. Energy Technol. (ICECET)*, Dec. 2021, pp. 1–6.

[9] A. M. Alex and J. Jacob, "Interfacial trap effect on the DC and RF characteristics of SiGe heterojunction bipolar transistor," in *Proc. Int. Conf. Commun., Control Inf. Sci. (ICCISc)*, vol. 1, Jun. 2021, pp. 1–5.

[10] X. Gao, G. Hennigan, L. Musson, A. Huang, and M. Negoita, "Simulation and investigation of electrothermal effects in heterojunction bipolar transistors," in *Proc. Int. Conf. Simulation Semiconductor Processes Devices (SISPAD)*, Sep. 2019, pp. 1–4.

[11] I. E. Getreu, *Modeling the Bipolar Transistor*. Amsterdam, The Netherlands: North Holland, 1978.

[12] P. J. Schubert and G. W. Neudeck, "Vertical bipolar transistors fabricated in local silicon on insulator films prepared using confined lateral selective epitaxial growth (CLSEG)," *IEEE Trans. Electron Devices*, vol. 37, no. 11, pp. 2336–2342, Nov. 1990.

[13] J. Warnock, P. F. Lu, T. C. Chen, and B. Meyerson, "Boron-doped emitters for high-performance vertical pnp transistors," in *Proc. Bipolar Circuits Technol. Meeting*, 1989, pp. 186–189.

[14] A. Hastings, *The Art of Analog Layout*, 2nd ed. Upper Saddle River, NJ, USA: Prentice-Hall, 2005.

[15] K. Kwon and I. Nam, "A linearization technique for a transconductor using vertical bipolar junction transistors in a CMOS process," *IEEE Trans. Microw. Theory Techn.*, vol. 61, no. 1, pp. 195–203, Jan. 2013.

[16] H. Klimach, A. Arnaud, C. Galup-Montoro, and M. C. Schneider, "MOSFET mismatch modeling: A new approach," *IEEE Design Test Comput.*, vol. 23, no. 1, pp. 20–29, Jan. 2006.

[17] N. Lu, "Modeling of distance-dependent mismatch and across-chip variations in semiconductor devices," *IEEE Trans. Electron Devices*, vol. 61, no. 2, pp. 342–350, Feb. 2014.

[18] P. G. Drennan, C. C. McAndrew, and J. Bates, "A comprehensive vertical BJT mismatch model," in *Proc. Bipolar/BiCMOS Circuits Technol. Meeting*, 1998, pp. 83–86.

[19] P. G. Drennan, C. C. McAndrew, J. Bates, and D. Schroder, "Rapid evaluation of the root causes of BJT mismatch," in *Proc. Int. Conf. Microelectron. Test Struct. (ICMTS)*, 2000, pp. 122–127.

[20] P. G. Drennan, "Device mismatch in BiCMOS technologies," in *Proc. Bipolar/BiCMOS Circuits Technol. Meeting*, 2002, pp. 104–111.

[21] M. Babazadeh, G. Johnson, J. Vickers, J. Estabil, N. Pakdaman, G. Steinbrueck, B. Borot, W. Doedel, and J. Galvier, "First look at across-chip performance variation using non-contact, performance-based metrology," in *Proc. 17th Annu. SEMI/IEEE ASMC Conf.*, 2006, pp. 278–283.

[22] X. Dong and L. Zhang, "Analog layout retargeting with process-variation-aware rule-based OPC," in *Proc. IEEE Int. Symp. Circuits Syst. (ISCAS)*, May 2017, pp. 1–4.

[23] A. Ghosh, R. M. Rao, C.-T. Chuang, and R. B. Brown, "On-chip process variation detection and compensation using delay and slew-rate monitoring circuits," in *Proc. 9th Int. Symp. Quality Electron. Design (ISQED)*, Mar. 2008, pp. 815–820.

[24] A. Ghosh, R. M. Rao, J.-J. Kim, C.-T. Chuang, and R. B. Brown, "On-chip process variation detection using slew-rate monitoring circuit," in *Proc. 21st Int. Conf. VLSI Design (VLSID)*, 2008, pp. 143–149.

[25] M. A. Hashem, "Analysis and design of BJT differential amplifier," in *Proc. 5th Int. Conf. Eng. Technol. Appl. (IICETA)*, May 2022, pp. 227–232.

[26] V. Gupta and G. A. Rincon-Mora, "Predicting and designing for the impact of process variations and mismatch on the trim range and yield of bandgap references," in *Proc. 6th Int. Symp. Quality Electron. Design (ISQED)*, 2005, pp. 503–508.

[27] S. Rodrigues and M. S. Bhat, "Impact of process variation induced transistor mismatch on sense amplifier performance," in *Proc. Int. Conf. Adv. Comput. Commun.*, Dec. 2006, pp. 497–502.

[28] S. Benali and H. Trabelsi, "Analysis of device mismatches effect on the performance of UWB-ring VCO," in *Proc. 17th Int. Multi-Conf. Syst., Signals Devices (SSD)*, Jul. 2020, pp. 814–818.

[29] Y. He, M. Choi, and Y.-B. Kim, "A compensation technique for threshold mismatch in sub-threshold current mirror," in *Proc. IEEE Microelectron. Design Test Symp. (MDTS)*, May 2021, pp. 1–4.

[30] P. Jain and B. P. Das, "On-chip threshold voltage variability detector targeting supply of ring oscillator for characterizing local device mismatch," in *Proc. IEEE 32nd Int. Conf. Microelectron. Test Struct. (ICMTS)*, Mar. 2019, pp. 120–125.

[31] M.-J. Chen and J.-S. Ho, "A three-parameters-only MOSFET subthreshold current CAD model considering back-gate bias and process variation," *IEEE Trans. Comput.-Aided Design Integr. Circuits Syst.*, vol. 16, no. 4, pp. 343–352, Apr. 1997.

[32] S.-C. Wong, K.-H. Pan, and D.-J. Ma, "A CMOS mismatch model and scaling effects," *IEEE Electron Device Lett.*, vol. 18, no. 6, pp. 261–263, Jun. 1997.

[33] J. J.-Y. Kuo, W. P.-N. Chen, and P. Su, "Investigation and analysis of mismatching properties for nanoscale strained MOSFETs," *IEEE Trans. Nanotechnol.*, vol. 9, no. 2, pp. 248–253, Mar. 2010.

[34] N. P. Maity, R. Maity, S. Maity, and S. Baishya, "Comparative analysis of the quantum FinFET and trigate FinFET based on modeling and simulation," *J. Comput. Electron.*, vol. 18, no. 2, pp. 492–499, Jun. 2019.

[35] D. Kim, S. Barraud, G. Ghibaudo, C. Theodorou, and J. W. Lee, "Drain current variability in 2-levels stacked nanowire gate all around P-type field effect transistors," in *Proc. 7th IEEE Electron Devices Technol. Manuf. Conf. (EDTM)*, Mar. 2023, pp. 1–3.

[36] T. E. A. Khan, S. Salini, G. M. Abraham, and T. A. S. Hameed, "Fin angle variation oriented threshold voltage model for a FDSOI FinFET," *IETE J. Res.*, vol. 68, no. 1, pp. 714–721, Jan. 2022.

[37] D. C. Ahlgren, B. Jagannathan, S.-J. Jeng, P. Smith, D. Angell, H. Chen, M. Khater, F. Pagette, J.-S. Rieh, K. Schonenberg, A. Stricker, G. Freeman, A. Joseph, K. Stein, and S. Subbanna, "Process variability analysis of a Si/SiGe HBT technology with greater than 200 GHz performance," in *Proc. Bipolar/BiCMOS Circuits Technol. Meeting*, 2002, pp. 80–83.

[38] G. Avenier, P. Chevalier, A. Montagné, L. Parmigiani, L. Berthier, O. Renault, E. Oghdayan, M. Mathieu, Y. Campidelli, D. Dutartre, and A. Chantre, "HBT device robustness against process variations in millimeter-wave BiCMOS technology," in *Proc. IEEE Bipolar/BiCMOS Circuits Technol. Meeting (BCTM)*, Sep. 2012, pp. 1–4.

[39] H. Holler, "Measurement and mismatch-modelling of semiconductor devices in BiCMOS technology," in *Proc. IEEE Int. Symp. Circuits Syst.*, vol. 4, May 2000, pp. 373–376.

[40] M. H. Abu-Rahma and M. Anis, "A statistical design-oriented delay variation model accounting for within-die variations," *IEEE Trans. Comput.-Aided Design Integr. Circuits Syst.*, vol. 27, no. 11, pp. 1983–1995, Nov. 2008.

[41] T. Poiroux, P. Scheer, A. Juge, and M. Vinet, "Multiscale statistically correlated variability: A unified model for computer-aided design," *IEEE Trans. Electron Devices*, vol. 62, no. 11, pp. 3605–3612, Nov. 2015.

[42] P. B. Y. Tan, C. C. Tan, and M. M. B. M. Fauzi, "Corner mismatch model for fast non-Monte Carlo best and worst cases simulation," in *Proc. IEEE Int. Conf. Semiconductor Electron. (ICSE)*, Aug. 2018, pp. 230–233.

[43] J. Gu, "Modeling method of local mismatch model for MOS transistors," in *Proc. China Semiconductor Technol. Int. Conf. (CSTIC)*, Shanghai, China, Jun. 2020, pp. 1–3.

[44] B. V. Benjamin, R. L. Smith, and K. A. Boahen, "An analytical MOS device model with mismatch and temperature variation for subthreshold circuits," *IEEE Trans. Circuits Syst. II, Exp. Briefs*, vol. 70, no. 6, pp. 1826–1830, Jun. 2023.

[45] K. Wu, N. Guo, F. Li, N. Zhu, J. Tao, and X. Li, "Efficient statistical parameter extraction for modeling MOSFET mismatch," *IEEE Trans. Comput.-Aided Design Integr. Circuits Syst.*, vol. 42, no. 5, pp. 1618–1622, May 2023.

[46] D. P. Kennedy, "Mathematical analysis of bipolar transistors," *IEEE Trans. Nucl. Sci.*, vol. NS-22, no. 6, pp. 2586–2594, Dec. 1975.

[47] G. D. Hachtel, M. H. Mack, R. R. O'Brien, and H. F. Quinn, "Two-dimensional finite element modeling of NPN devices," in *IEDM Tech. Dig.*, 1976, pp. 166–169.

[48] H. Cho and D. E. Burk, "The modeling and measurement of lateral bipolar junction transistors," in *Proc. Bipolar Circuits Technol. Meeting*, 1991, pp. 93–96.

[49] K. Joardar, "A new approach for direct observation of base width modulation in vertical bipolar transistors," *IEEE Trans. Electron Devices*, vol. 42, no. 12, pp. 2189–2196, Dec. 1995.

[50] R. C. Jaeger, S. Hussain, J. C. Suhling, P. Gnanachchelvi, B. M. Wilamowski, and M. C. Hamilton, "Impact of mechanical stress on bipolar transistor current gain and early voltage," in *Proc. IEEE SENSORS*, Nov. 2013, pp. 1–4.

[51] C. Compton, "NPN mismatch dependence on layout," in *Proc. IEEE Int. Conf. Microelectron. Test Struct. (ICMTS)*, Mar. 2018, pp. 102–107.

[52] M. J. M. Pelgrom, A. C. J. Duinmaijer, and A. P. G. Welbers, "Matching properties of MOS transistors," *IEEE J. Solid-State Circuits*, vol. 24, no. 5, pp. 1433–1439, Oct. 1989.
[53] C. Michael and M. Ismail, "Statistical modeling of device mismatch for analog MOS integrated circuits," *IEEE J. Solid-State Circuits*, vol. 27, no. 2, pp. 154–166, Feb. 1992.
[54] C. J. Abel, C. Michael, M. Ismail, C. S. Teng, and R. Lahri, "Characterization of transistor mismatch for statistical CAD of submicron CMOS analog circuits," in *Proc. IEEE Int. Symp. Circuits Syst.*, vol. 2, May 1993, pp. 1401–1404.

**XIAONIAN LIU** received the B.Sc. degree in physics from Fudan University, Shanghai, China, in 2013, and the Ph.D. degree in microelectronics and solid state electronics from the University of Chinese Academy of Sciences, Beijing, China, in 2018.

From 2018 to 2020, he was a lead Software Engineer with Shanghai Cadence Electronics Technology Company Ltd., for the development of physical implementation tool Innovus. Since 2020, he has been a Lecturer with the School of Physics and Electronics, Hunan Normal University, Changsha, China. His research interests include the semiconductor devices modeling, the radiation effects of integrated devices and circuits, and the physical placement algorithms of VLSI.

**ZICHEN YANG** received the B.Tech. degree in communication engineering from the College of Computer and Electrical Engineering, Hunan University of Arts and Science, Changde, China, in 2021. She is currently pursuing the M.Tech. degree with the School of Physics and Electronics, Hunan Normal University, Changsha, China.

She has attended and delivered an oral presentation on 2023 7th International Conference on Robotics and Automation Sciences (ICRAS 2023). Her research interests include integrated devices and circuits, especially the reliability of semiconductor devices and the high speed digital circuits design.